

Performance Estimates for the Giant Magellan Telescope via Statistical Analysis

Breann N. Sitarski*^a, Konstantinos Vogiatzis^a, Rod Conan^a, George Angeli^a, Bob Goodrich^a

^aGiant Magellan Telescope Organization, 465 N. Halstead St., Pasadena, CA 91107, USA

ABSTRACT

System performance estimates are stochastic processes with contributions from random effects and predictable actions. One of the random effects and design drivers of large, ground-based observatories like the Giant Magellan Telescope (GMT) is the environment in which the observatory will exist. The Stochastic Framework that facilitates estimates of system performance relies on a historical, multi-year record of environmental data. The multi-year record, along with models of the observatory, are used in a Monte-Carlo analysis to estimate performance parameters such as dome seeing and wind jitter effects that inform both observatory design and active and adaptive optics performance.

Environmental, atmospheric, and telescope orientation data can be used and propagated through a one-dimensional thermal model of the enclosure for first-order flux boundary conditions used to inform computational fluid dynamics (CFD) modeling. The results from dome seeing and wind jitter are integrated over our 400-second simulation time span in order to give estimates of time-integrated image quality performance. This paper describes the data the feeds into the 1D thermal model, the 1D thermal model itself, and how the CFD results are used to determine the median image quality value from dome seeing and wind jitter over the length of the data record, the “Standard Year.” The image quality metrics are folded directly into the image quality budgets that are also presented in this conference.

Keywords: Image quality, environmental conditions, dome seeing, modeling

1. A STOCHASTIC FRAMEWORK FOR PERFORMANCE ESTIMATES

The 25.4-meter Giant Magellan Telescope (GMT) is part of the next generation of extremely large telescopes (ELTs) that are set to have first light within the next decade. It will be located at Las Campanas Peak, one of the best natural seeing sites in the world with a median seeing of 0.63 arcseconds in the V-band. The primary aperture has an aplanatic Gregorian design, which is useful for canceling low-order aberrations. The entrance aperture consists of seven 8.4-meter diameter segments that are perfectly conjugated to 7 segmented, 1.05-meter secondary mirror segments. Two secondary mirrors are currently planned: a fully adaptive secondary mirror conjugated to the ground layer of the atmosphere to facilitate excellent Ground Layer Adaptive Optics correction and will be used for Natural Guide Star and Laser Tomographic Adaptive Optics, and a fast-steering secondary mirror that will allow for piston, tip, and tilt for natural seeing modes when the adaptive secondary is undergoing maintenance. The optical design of GMT enables large fields of view (up to 20 arcminutes in diameter), and its compact f/8 focus gives a ~ 1 arcsecond/mm plate scale that equates to fairly compact instruments for an ELT. For more information about GMT, see Fanson et al. (2018)¹.

GMT is developing a series of error budgets to estimate the performance of the entire Observatory. The performance is dependent on: deterministic effects (i.e., optical design residual); deterministic effects that are randomized by the environmental and operational parameters; random effects such as wind buffeting, thermal seeing, atmospheric seeing, and actuator and sensor noise; and material, fabrication, and installation errors. All of these can be taken into account and the observatory performance can be characterized as a statistical variable dependent on the observing environment.

Random effects can be taken into account via a historical record of site survey data originally taken for site selection (2005 – 2008; Thomas-Osip et al. 2011²). The environmental conditions were monitored and records were taken of wind speed, wind direction, dry bulb temperature, dew point temperature, humidity, cloud cover, and atmospheric turbulence via a MASS/DIMM system. See Section 2 for more details.

Image quality is an example of a statistical variable that needs to be hardy against outliers as just a few points in the image

*bsitarski@gmto.org; phone 1 626 204-0500 x 5233; <http://gmto.org>

quality distribution do not fully constrain performance. For our purposes, we use statistical over **all** environmental and operational conditions (i.e., telescope pointing angle) to characterize performance, and the median of the image quality over all conditions is constrained as the requirement. This is a natural and evolving verification method for AIVC. For more information on similar frameworks, see Voigtatzis et al. (2019)³ and Angeli and Vogiatzis (2010)⁴. A model for the statistical framework is given in Figure 1 below. Each step will be described in more detail in the following sections.

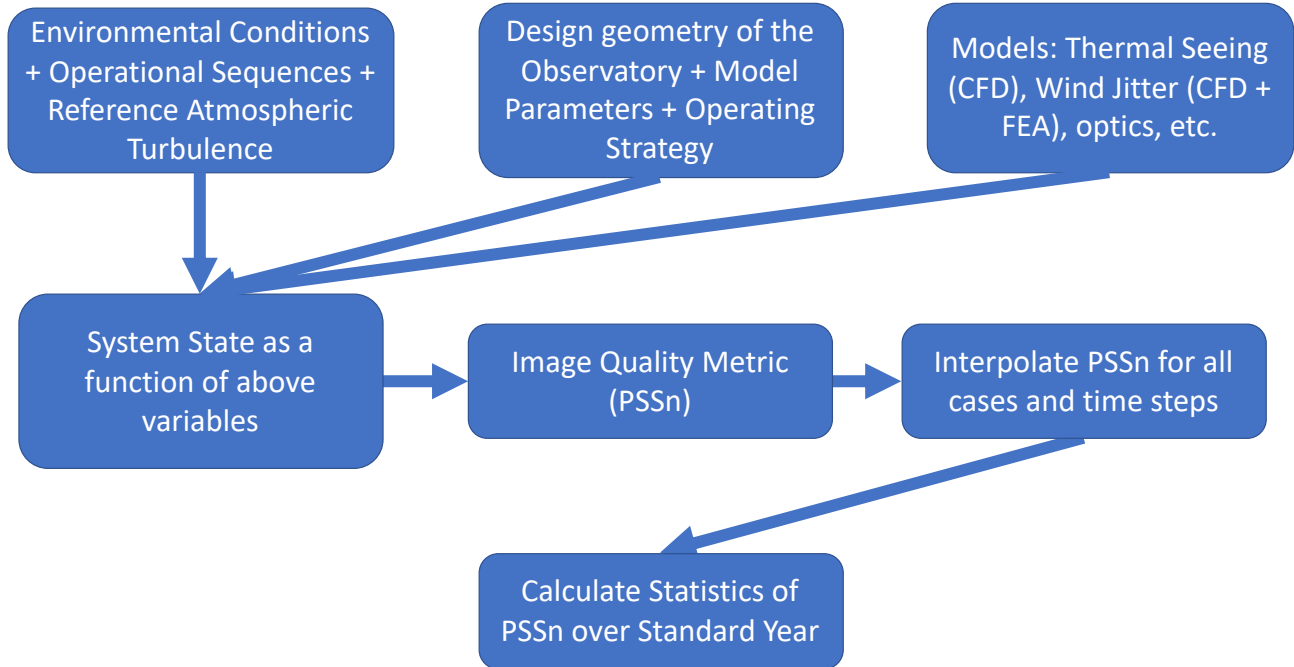


Figure 1: Flow for stochastic framework for characterizing the observatory performance as a statistical variable dependent on the observing environment.

The metric used for evaluating the image quality the Normalized Point Source Sensitivity (PSSN; Seo et al. 2009⁵; Angeli et al. 2011⁶). The PSSN reflects the science capability and efficiency of the observatory and is inversely related to the equivalent noise area. PSSN relates the actual performance of the system to a reference, typically the equivalent noise area of the representative atmosphere of the site with a perfect telescope. The PSSN is given by:

$$PSSN = \frac{\iint |PSF_{a+t+e}|^2}{\iint |PSF_{a+t}|^2}$$

where PSF_{a+t+e} is the time-averaged PSF of the atmosphere and aberrated telescope while PSF_{a+t} is the time-averaged PSF of the atmosphere and perfect telescope.

For practical optical errors, the PSSN is a multiplicative value to a good approximation. Figure 2 below shows the combined vs. multiplied PSSN values. The combined PSSN is derived from the sum of wavefront errors for a series of primary mirror errors after 27 bending mode correction from the active optics system. The multiplicative and combined errors are nearly identical, implying that independent PSSN values can be multiplied together to derive total PSSN error.

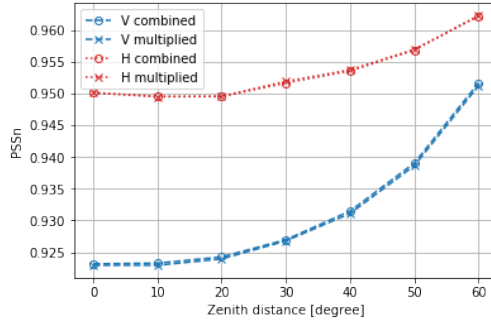


Figure 2: Combined vs. multiplied PSSN values.

2. ENVIRONMENTAL HISTORICAL RECORD: THE GMT SITE SURVEY

The heart of the stochastic framework includes a historical record of environmental and operational conditions at the selected GMT site. During site selection, a number of Davis weather stations were deployed at various locations in the Chilean Andes. The selected GMT site ($29^{\circ}02'55.26''\text{S}$, $70^{\circ}40'56.00''\text{W}$ at 2514 m elevation) had such a weather station located from September 2005 – December 2009 that recorded environmental data such as temperature, wind speed, barometric pressure, and wind direction. A Differential Image Motion Monitoring (DIMM) station at a 7- meter height was also deployed at the current GMT site during the same period, allowing us to simultaneously collect turbulence data and environmental records. A Multi-Aperture Scintillation Sensor (MASS) station was located less than 5 km from the site, and we adopt the values here for the GMT site as the free atmosphere above 50 m will likely be the same between the two sites. For more information on the site survey, see Thomas-Osip et al. (2011)².

Telescope pointing data is also an essential component to determine relative azimuths between the wind and the telescope operating position. As GMT has not yet been constructed, we use telescope pointing data taken between April 2011 and April 2014 from the Magellan Baade telescope as a representation of where the GMT might point in the future. As this pointing data unfortunately does not align in time with our environmental history record, we assume that the telescope pointing behavior in 2011-2014 would be the same as that during the environmental data collection. That is, the data were matched to the proper day (i.e., October 14, 2011 was matched to October 14, 2005) and the data were repeated to match the entire time span. While this is not the most reliable process as it does not tie observational behavior directly to weather (i.e., observations may still go on in this way even if weather conditions are poor), it does provide us with some data and some background so that we can establish our metrics. Data is currently being taken at the GMT site with Vaisala weather stations, which have better accuracy and precision levels than the Davis weather stations. A DIMM system was also recently commissioned and fully automated up at the summit; these two sets of records, combined with Magellan pointing data, could provide additional standard year data in the future.

The data are nearest-neighbor interpolated over a 2-minute time step that was dictated by the availability of data (1 – 2 minute sampling rate of the weather stations, DIMM, and MASS data; 30-second sampling of telescope orientation) and the compatibility with the enclosure thermal model time step (as the telescope-enclosure orientation can be considered fixed during the 2 minute timeframe).

Examples of the distributions of the environmental conditions are given in Figure 3 below. The temperature and wind speed distributions show night only (science operating conditions) and night and day (all operating conditions) within the distributions. The center distribution in the third row shows the seeing from the DIMM site and further shows the excellent natural seeing conditions of the site. The second-to-last row shows the telescope operational history. The third column has two-dimensional histograms. It is noteworthy that for the 2D histograms that contain seeing data, most of the DIMM values that are recorded are between 0.5 and 0.8 arcseconds, so any perceived correlations are inconclusive.

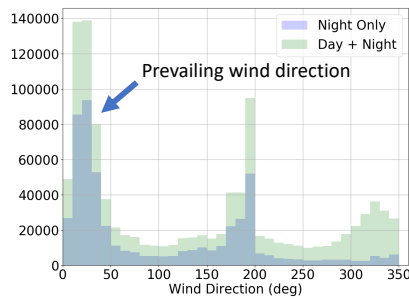
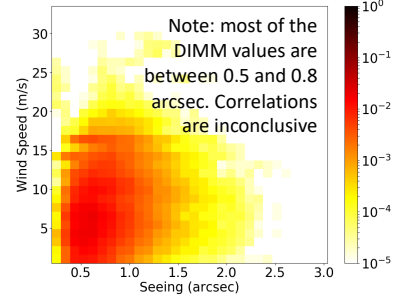
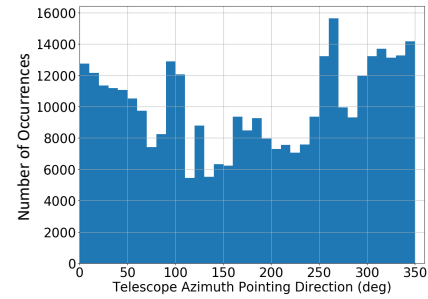
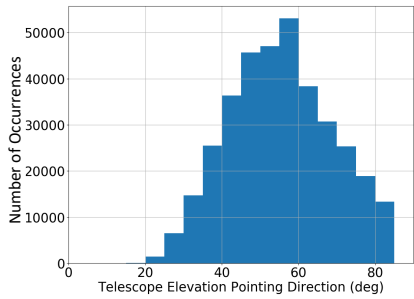
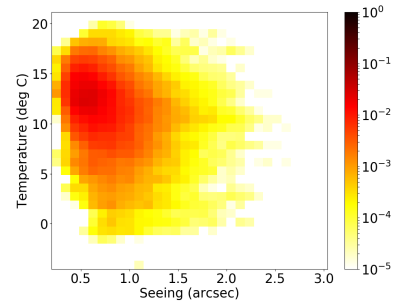
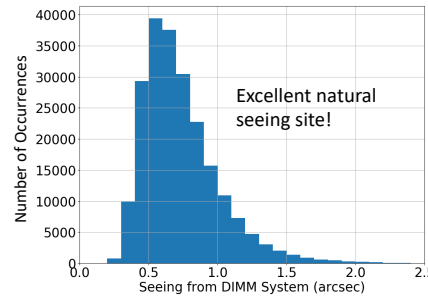
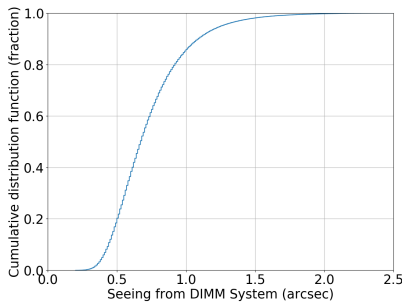
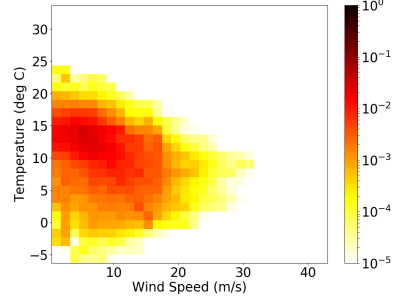
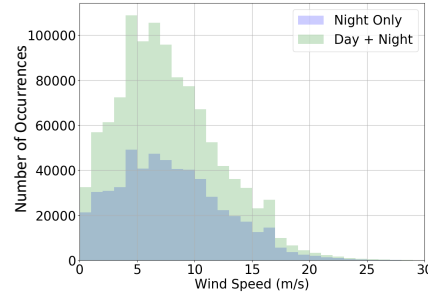
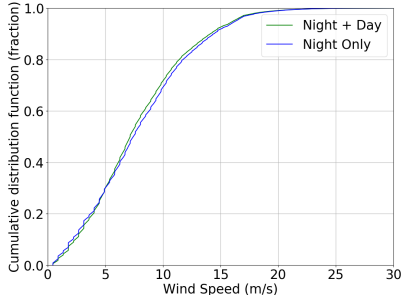
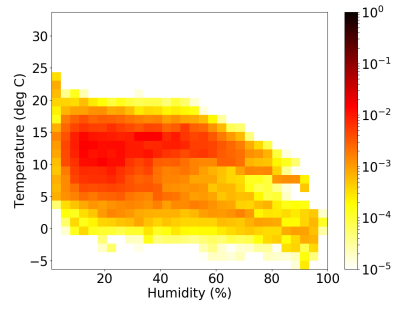
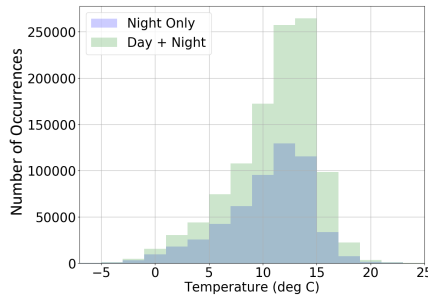
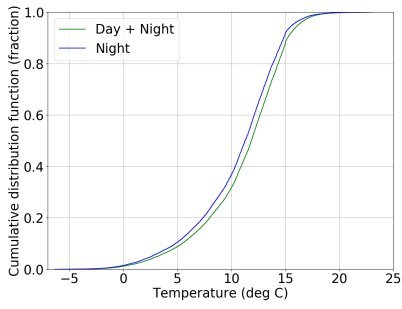


Figure 3: Cumulative and probability distribution functions for various environmental and operational parameters. All are included, among others, in the standard year framework that are used to model performance.

3. APPLICATIONS TO SIMULATIONS

3.1 Dome seeing

One of the largest terms in the natural seeing image quality error budget is dome seeing (see Sitarski et al.⁷, this conference, and Conan et al., this conference⁸). In order to quantify how much dome seeing will affect observatory performance, computational fluid dynamics (CFD) simulations were run for 400 seconds at various relative telescope-to-wind direction azimuths and wind speeds (e.g., Vogiatzis et al. 2018,⁹ Das et al. 2018¹⁰). Changes in the refractive index at each time step were ray-traced to the exit pupil of the telescope and the optical path difference at each wind speed and enclosure orientation was used to compute the PSSN at each time step and integrated over the entire time frame. A look-up table was then generated and interpolated over the entire standard year data set for the reference atmosphere ($r_0 = 16$ cm at a zenith angle of 0°). One compelling aspect of using CFD analysis is that changes in the refractive index and other parameters, including the forces on various nodes in the model and wind jitter, can be determined at each time step as well; statistics on various parameters can therefore be computed over the standard year. Inputs to the CFD model include the enclosure and mount design, which can be used to optimize various aspects of both structures, including vent configuration, secondary support truss geometry, etc.

Figure 4 below shows a snapshot from one of the Standard Year CFD modeling cases. The left-hand side of Figure 5 shows the mean thermal seeing as a function of wind speed over the standard year. The orange points represent a deployed wind screen, while the blue points represent an open wind screen. Note that the thermal seeing is the worst at low wind speeds due to a lack of flushing. The right-hand side of Figure 5 shows the cumulative distribution function of the GMT thermal performance over the standard year. Each point that has valid data over the standard year is nearest-neighbor interpolated to a representative case where a CFD simulation has been run (as a function of wind speed and wind direction). Future work will be to use a similar framework to estimate other image quality error budget terms. The enclosure structure design is currently being updated so more results are forthcoming.

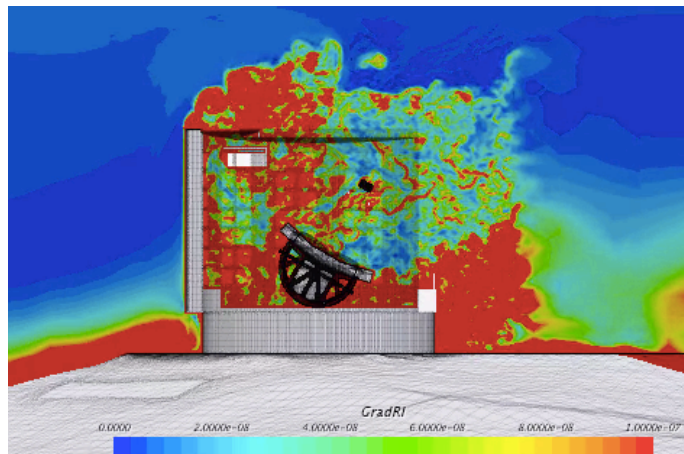


Figure 4: Snapshot of CFD simulation.

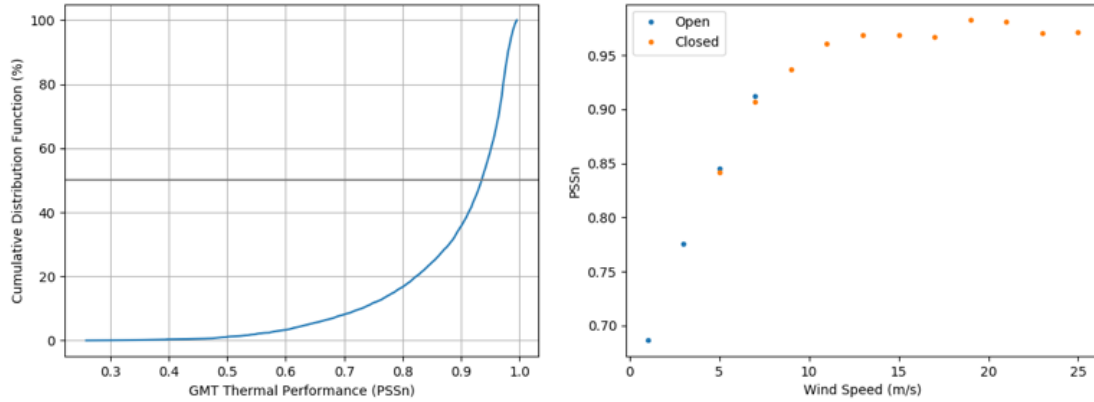


Figure 5: *Left*: GMT thermal performance over the standard year. *Right*: PSSn as a function of wind speed. Each point represents the mean in the bin.

3.2 1D Lumped-Mass Enclosure Model for HVAC Optimization

The goal with this simulation was to obtain an estimate for a moderately-sized HVAC system that will keep the structures in the Enclosure to within 0.5 K from the ambient temperatures, following the requirements in the Observatory Architecture Document (OAD). This is a simplified one-dimensional model that computes the temperature differences between the enclosure surfaces, the telescope structure, and ambient air required for applied boundary conditions in the CFD simulations. As this model works to produce information to inform the CFD models, the calculation needs to run quickly for comparisons.

The model itself uses a 1D transient heat conduction equation and uses fluxes for the boundary conditions (Vogiatzis et al. 2019³; see Figure 6):

$$\frac{\partial T}{\partial t} = \frac{k}{\rho c_p} \frac{\partial^2 T}{\partial z^2}, \quad -k \frac{\partial T}{\partial z} = q_{boundaries}$$

The primary input for the 1D lumped-mass model is the historical environmental conditions record from the standard year. This includes the relative humidity, temperature, time stamps, wind speed, relative azimuth of observations and wind directions. Any gaps in the environmental data are linearly interpolated over (i.e., in the case that there is no temperature data for a given epoch). Additional inputs are the thermal properties of the structure, the diameter and height of the enclosure, a solar flux calculation, an infiltration model (Sherman & Grimsrud 1980¹¹), interior heat load estimation, air conditioning efficiency, target temperature, nozzle temperature estimates, and flow rate of the air conditioning system. A sky temperature was also estimated for radiation terms via the Berdahl & Martin (1984)¹² model with constants from NOAA. The temperature at each node is computed to be used for CFD boundary conditions, and statistics over the standard year are obtained for each simulation run. The simulation itself is modular and versatile and can be easily and quickly adjusted to look at various conditions and parameters. For example, several of our runs used different infiltration models; others had periods without HVAC to investigate the extreme temperatures in the enclosure in case the HVAC system malfunctioned. Others included two-week long closures for maintenance, both with and without HVAC.

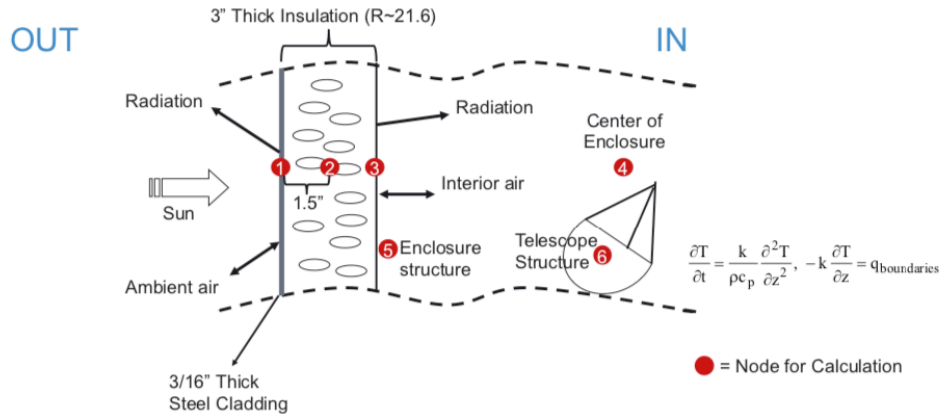


Figure 6: Computational nodes for HVAC simulations.

Figure 7 shows the diurnally-averaged and azimuthally-averaged temperatures modeled over the standard year. “117” identifies a simulation with an efficient HVAC system (capacity = 175000 CFM; $T_{\text{nozzle}} = T_{\text{target}} - 1$, and T_{target} is the median forecasted temperature of the night). “str” refers to the telescope structure; “enc” refers to the enclosure structure; “in” is the computed interior ambient temperature; “clad” is the temperature of the enclosure outer skin; “node 3” is the node next to the insulation between the outer cladding and the inner interior wall of the enclosure; and the “outside ambient” is the reported dry bulb temperature for comparison. This includes an infiltration model and heat transfer coefficients for the telescope structure and enclosure structure based on CFD simulations. “118” refers to a simulation without any HVAC system (i.e., HVAC efficiency = 0.0). The effect of no HVAC system on the interior of the enclosure is readily apparent.

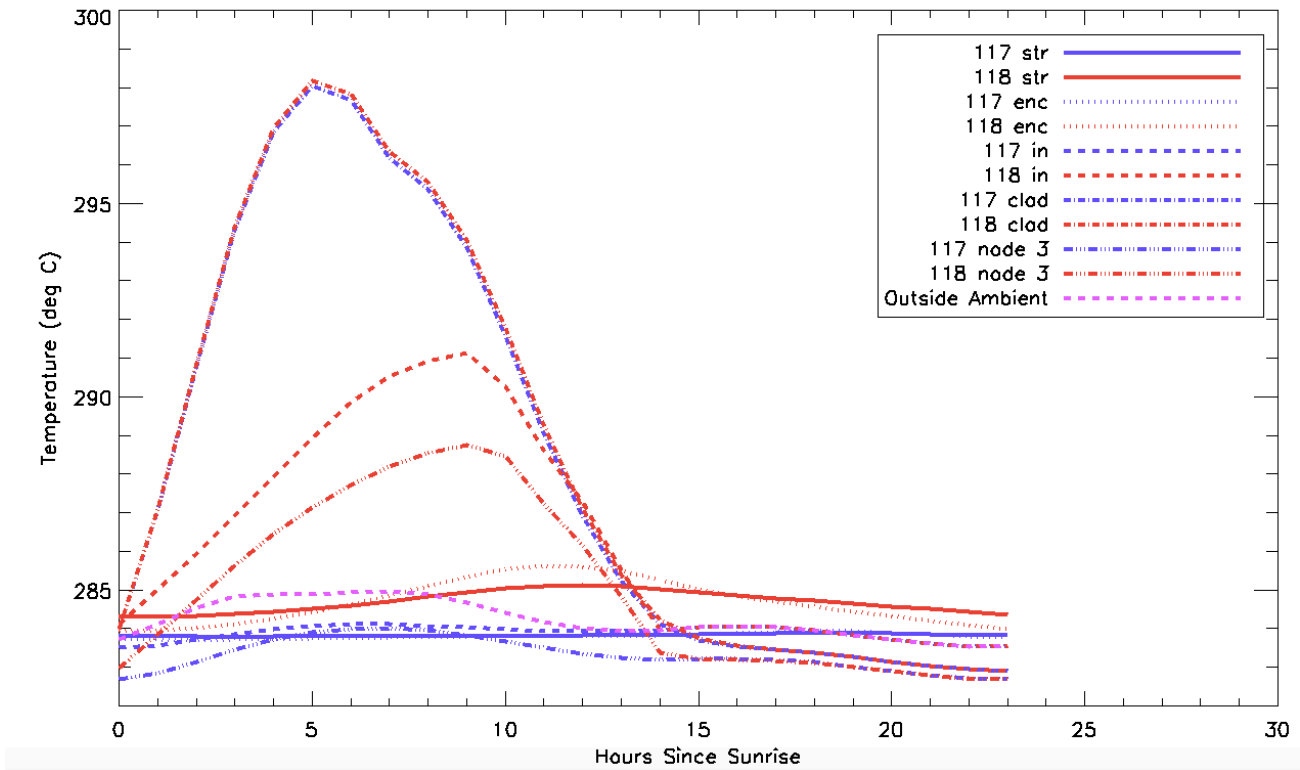


Figure 7: Diurnally-averaged and azimuthally-averaged temperatures at various conditions modeled over the standard year.

4. FUTURE WORK

As discussed above, the standard year stochastic framework is useful for obtaining statistics on observatory performance estimates. Future work is to adapt this framework for other image quality error budget terms that vary with environmental and operational conditions. As the design for various aspects of the enclosure and the telescope evolve, models will be updated and the framework reran to see the effects (see Figure 1).

- [1] Fanson, J., McCarthy, P., Bernstein, R., Angeli, G., Ashby, D., Bigelow, B., Bouchez, A., Burgett, W., Chauvin, E., Contos, A., Figueroa, F., Gray, P., Groark, F., Laskin, R., Millan-Gabet, R., Rakich, A., Sandoval, R., Pi, M., Wheeler, N., "Overview and Status of the Giant Magellan Telescope project," Proc. SPIE 10700, Ground-Based and Airborne Telescopes VII, 1070012 (2018).
- [2] Thomas-Osip, J., Prieto, G., Johns, M., Phillips, M. M., "Giant Magellan Telescope site evaluation and characterization at Las Campanas Observatory," Proc. SPIE 7012, Ground-Based and Airborne Telescope II, 70121U (2008).
- [3] Vogiatzis, K., Das, K., Sitarski, B., Schwartz, D., Conan, R., Angeli, G., "Using a Stochastic Approach to Estimate the Aerothermal Performance of the Giant Magellan Telescope," Proc. AIAA, Unstead Aerodynamics III, AIAA 2019-2319 (2019).
- [4] Angeli, G., Vogiatzis, K., "Statistic approach to systems engineering for the Thirty Meter Telescope," Proc. SPIE 7738, Modeling, Systems Engineering, and Project Management for Astronomy IV, 773817 (2010).
- [5] Seo, B.-J., Nissly, C., Troy, M., Angeli, G., "Analysis of normalized point source sensitivity as a performance metric for large telescopes," Applied Optics, 48, 31 (2009).
- [6] Angeli, G. Z., Seo, B.-J., Nissly, C., Troy, M., "A convenient telescope performance metric for imaging through turbulence," Proc. SPIE 8127, Optical Modeling and Performance Predictions V, 812709 (2011).
- [7] Sitarski, B. N., Vogiatzis, K., Conan, R., Angeli, G. Z., Goodrich, B., "Performance Estimates for the Giant Magellan Telescope via Statistical Analysis," this conference.
- [8] Conan, R., et al., "Modeling the Giant Magellan Telescope dome seeing using fluid dynamics simulations," This conference.
- [9] Vogiatzis, K., Das, K., Angeli, G., Bigelow, B., Burgett, W., "Computational fluid dynamics modeling of GMT," Proc. SPIE 10705, Modeling, Systems Engineer, and Project Management for Astronomy VIII, 107050R (2018).
- [10] Das, K., Vogiatzis, K., Angeli, G., Rosenthal, W., Bouchez, A., Goodrich, R., Sitarski, B., "GMT aerothermal modeling validation through site measurements," Proc. SPIE 10705, Modeling, Systems Engineering, and Project Management for Astronomy VIII, 1070502 (2018).
- [11] Sherman, M. H., and Grimsrud, D. T., "Infiltration-Pressurization Correlation: Simplified Physical Modeling," Proc. American Society of Heating, Refrigeration, and Air Conditioning Engineers (1980).
- [12] Berdahl, P., and Martin, M., "Emissivity of clear skies," Solar Energy, 32, 5, 663 (1984).